Noncanonical interactions and conformational dynamics in cargo-Pex5-Pex14 ternary complex for peroxisomal import

Ravi R. Sonani[1,$], Artur Blat[1,2], Małgorzata Jemioła-Rzemińska[3], Oskar Lipiński[1,2], Stuti N. Patel[1], Tabassum Sood[1,2], Grzegorz Dubin[1,#]

[1] Malopolska Centre of Biotechnology, Jagiellonian University, Krakow, Poland

[2] Doctoral School of Exact and Natural Sciences, Jagiellonian University, Krakow, Poland

[3] Faculty of Biochemistry, Biophysics and Biotechnology, Jagiellonian University, Krakow, Poland

[$]Current Address: Department of Biochemistry and Molecular Genetics, University of Virginia School of Medicine, Charlottesville, VA 22903, USA

[#] correspondence to: grzegorz.dubin@uj.edu.pl

ABSTRACT

Peroxisomes are membrane bound organelles which compartmentalize diverse metabolic processes in eukaryotic cells. Having no protein synthetic abilities, peroxisomes import all required enzymes from the cytosol through a peroxin (Pex) import system. In the first step, the Peroxisome Targeting Sequence 1 (PTS1)-marked cargo is recognized by soluble receptor, Pex5. The cargo-Pex5 complex then docks at the peroxisomal membrane translocon containing Pex14 and Pex13 and translocates into peroxisomal lumen, but the structural understanding is elusive. Here, we report a cryo-EM structure of cargo-Pex5-Pex14 ternary complex from *Trypanosoma cruzi,* the causative agent of human Chagas disease. Malate dehydrogenase (cargo) – Pex5 interface is characterized by a swinging motion of Pex5 restricted by secondary, PTS1 independent interactions. The Pex5-Pex14 interface reveals a noncanonical contact surface adjacent to the previously identified Wxxx(F/Y) motif. Mutational analysis demonstrates that noncanonical interactions did not evolve to increase the affinity, but rather to restrict the dynamics at the cost of affinity. Consequences for the peroxisomal transport are discussed.

HIGHLIGHTS

1. The structure of a ternary complex (MDH-Pex5-Pex14) enabling cargo translocation *via* peroxisomal membrane was determined using cryo-EM.

2. Pex5 interface with the cargo (MDH) is characterized by significant conformational dynamics restricted by PTS1 independent interactions

3. Wxxx(F/Y) motif mediated docking of Pex14 at Pex5 is complemented by interactions at the noncanonical site.

INTRODUCTION

Peroxisomes compartmentalize a set of important metabolic processes in eukaryotic cells including catabolism of fatty acids and polyamines, biosynthesis of ether phospholipids, glyoxylate cycle in germinating seeds, glycolysis in *Typanosoma* and many other (*1, 2*). Peroxisomes lack genetic material and protein synthetic ability and import the required enzymes (cargo) from the cytoplasm (*3*). The import system comprises more than a dozen peroxins (Pex) which recognize peroxisomal targeting signal (PTS) sequence on folded cargo proteins in the cytoplasm, translocate the cargo into the peroxisomal lumen and recycle the Pex system for following rounds of cargo import (*4*). Interestingly, translocation *via* the Pex system does not require cargo unfolding.

The initial step of the transport involves recognition of a more common PTS1 signal by soluble Pex5 receptor in the cytoplasm. The less common PTS2 signal requires additional interaction with Pex7. PTS1 comprises of three C-terminal residues characterized by Ser-Lys-Leu-COOH consensus sequence (*4*). It is recognized by a soluble receptor - Pex5 through its C-terminal tetratricopeptide repeat (TPR) domain. Crystal structures of isolated TPR domain and short peptides encompassing PTS1 show that the signal peptide anchors at a deep central cavity of TPR. The interaction is stabilized by a network of hydrogen bonds involving the C-terminal carboxylate group, the mainchain donors and acceptors and lysine sidechain amine (*5*). Single available structure of a full length cargo in complex with Pex5 TPR domain suggests that secondary interactions may modulate the PTS1 driven binding (*6-8*), but the question of a general character of the secondary interactions remains unresolved and awaits broader structural characterization.

The translocation of Pex5-cargo complex through the peroxisomal membrane is assisted by Pex13 and Pex14. Pex13 forms a matrix of the import pore enabling diffusion of Pex5-cargo complex (*9*). Peroxisomal membrane spanning Pex14 facilitates docking of Pex5-cargo complex at the cytoplasmic side and release at the peroxisomal lumen.

Canonical interaction of Pex14 and Pex5 involves recognition of several Wxxx(F/Y) motifs within the N-terminal domain of Pex5 (Pex5 NTD) by N-terminal globular domain of Pex14 (Pex14 NTD) (*10-13*). The binding is documented by a structure of Pex14 NTD bound to short Pex5 fragment encompassing the Wxxx(F/Y) motif (*14*). The motif folds into an

amphipathic helix where the aromatic sidechains occupy two shallow pockets at the surface of Pex14, while the helix protects the binding site from unfavorable solvent interactions (*14*).

An ongoing controversy regards the topology of Pex14 in the peroxisomal membrane. Some studies suggest that the Pex14 NTD faces the cytoplasm while other indicate it locates in the peroxisomal lumen (*15-22*). The former orientation would imply that Wxxx(F/Y) motifs are utilized for cargo docking at the peroxisomal membrane while the latter suggests their possible role in cargo release.

Regardless the membrane orientation of Pex14, the cooperation of multiple copies of Wxxx(F/Y) motif in Pex5 in binding Pex14 is poorly understood (*10-13*). Low resolution studies suggested that the largely unstructured N-terminal domain of Pex5 folds into a stable scaffold upon saturation with Pex14 NTDs (*23*). This observation is interesting in the light of a recent cryo-EM structure of full length Pex14 where a large rod-like coiled coil domain of Pex14 homotrimer is well resolved (*24*), but the Wxxx(F/Y) binding domains located at the other side of the peroxisomal membrane, are not resolved. This suggests no cooperation of Wxxx(F/Y) binding domains within Pex14 trimer, but interaction of Pex5 may possibly result in rigidification of the complex.

To address the role of secondary interactions in cargo-Pex5 complex and to assess the presumed folding of Pex5 NTD in the presence of Pex14 we determined the structure of ternary complex containing cargo loaded full-length Pex5 saturated with Pex14. We selected *Trypanosoma cruzi* as a model organism because of the significance of peroxisomal transport in this agent of human Chagas disease (*25*), and comparable organization of initial translocation steps in *Trypanosoma* and mammals.

RESULTS AND DISCUSSION

Reconstitution of *Trypanosoma cruzi* cargo-Pex5-Pex14 ternary complex

Having evaluated a number of cargo proteins and Pex constructs, we have selected peroxisomal (glycosomal) malate dehydrogenase (MDH) containing complex for structural analysis. Full length Pex5 (residues 1-666, GenBank acc. no. PBJ69826.1), N-terminal domain

of Pex14 (residues 21-85, GenBank acc. no. RNC55913.1) and MDH (residues 1-323, UniProt id: Q4DRD8) were individually expressed in *E. coli* and purified to homogeneity. The complex was reconstituted by mixing and separated from remaining individual components by size exclusion chromatography. The presence of all components in samples used for cryo-EM grid preparation was evaluated by SDS-PAGE and the samples were characterized by supplementary methods consistently supporting complex formation (Supplementary Figure S1).

Compositional and conformational heterogeneity of the sample

Initial processing of cryo-EM data revealed a consistently homotetrameric arrangement of MDH particles, but substantial heterogeneity in stoichiometries of the complex with Pex5. We avoided chemical crosslinking which could possibly shift the equilibrium into a more homogenous population, but rather extracted the information on compositional heterogeneity from available data. Relevant classification allowed to reconstruct 3D volume maps for compositionally diverse complexes, showing prominent density for a single Pex5 molecule (hereafter MP1), two copies of Pex5 (MP2) and three copies of Pex5 (MP3) bound to the MDH tetramer (Fig. 1, Supp. Fig. S2). The density of the third copy of Pex5 in MP3 is week and scattered and the complex with four copies of Pex5 was not observed (Supp. Fig. S2). These results suggest that at the conditions used in the experiment MDH tetramer exists in an unsaturated equilibrium with Pex5. Because saturated MDH:Pex5 stoichiometry was maintained during sample preparation, partial dissociation is most likely induced during grid preparation.

Initial attempts at obtaining 3D volume maps of MP1, MP2 and MP3 by standard data-processing pipeline resulted in density maps having well-resolved MDH region and poorly resolved Pex5 regions, suggesting conformational heterogeneity of the latter component. Already at this point, the density for MDH allowed model fitting with high confidence using a crystal structure of MDH determined here in complex with NAD^+ cofactor (PDB ID: 7QOZ). In the cryo-EM map, MDH exists as a tetramer of ~10nm diameter, which is consistent with MALS and DLS data (Supp. Fig. S1), and the crystal structure. Peroxisomal transport signal 1 (PTS1) of all MDH protomers are positioned at the periphery of the MDH-tetramer and are equally accessible.

In order to interpret the conformational heterogeneity in the Pex-region of the complex, three-dimensional variability analysis (3DVA) was employed (*26*). The analysis identified a significant swinging movement of Pex5 relative to MDH (Suppl. Movies 1 and 4). By using clustered particles, we could reconstruct a number of conformationally discrete 3D volumes representing the snapshots of the swinging motion. We have refined and built two exemplary structures for both MP1 and MP2 complex, representing two extreme conformations (close and distal) of the swinging (hereafter MP1-c, MP1-d, MP2-c and MP2-d) (Fig. 1; Suppl. Movies 2, 3, 5, 6 and 7). The refined maps show features sufficient for atomic model building of MDH and Pex5 TPR domain along with an upstream helix (residues 328-358), not resolved in available crystal structures of Pex5 TPR domain (Supp. Figs. S3-S7). Additional poorly-resolved density visible around the Wxxx(F/Y) motif proximal to the TPR domain of Pex5 could account either for the remaining Pex5 NTD or Pex14. To address this, we have reconstituted the complex using Pex5 variant (residues 314-666) which is devoid of NTD while retaining the Wxxx(F/Y) motif proximal to the TPR domain (*12*), and solved its cryo-EM structure. The resultant map displayed the density around the Wxxx(F/Y) motif indicating that this density potentially accounts for Pex14 (Supp. Fig. S11).

The maps obtained for a complex containing full length Pex5 show no density for Pex5 NTD. Such observation suggests a flexible nature of Pex5 NTD relative to the TPR domain since the presence of full length Pex5 in our samples was confirmed by SDS-PAGE directly before grid preparation and saturation with Pex14 was ensured by stoichiometry. The result corresponds with the earlier studies suggesting the unstructured character of apo Pex5 NTD (*27*), but is inconsistent with the earlier report suggesting the rigidification of the N-terminal part of Pex5 upon Pex14 binding (*23*).

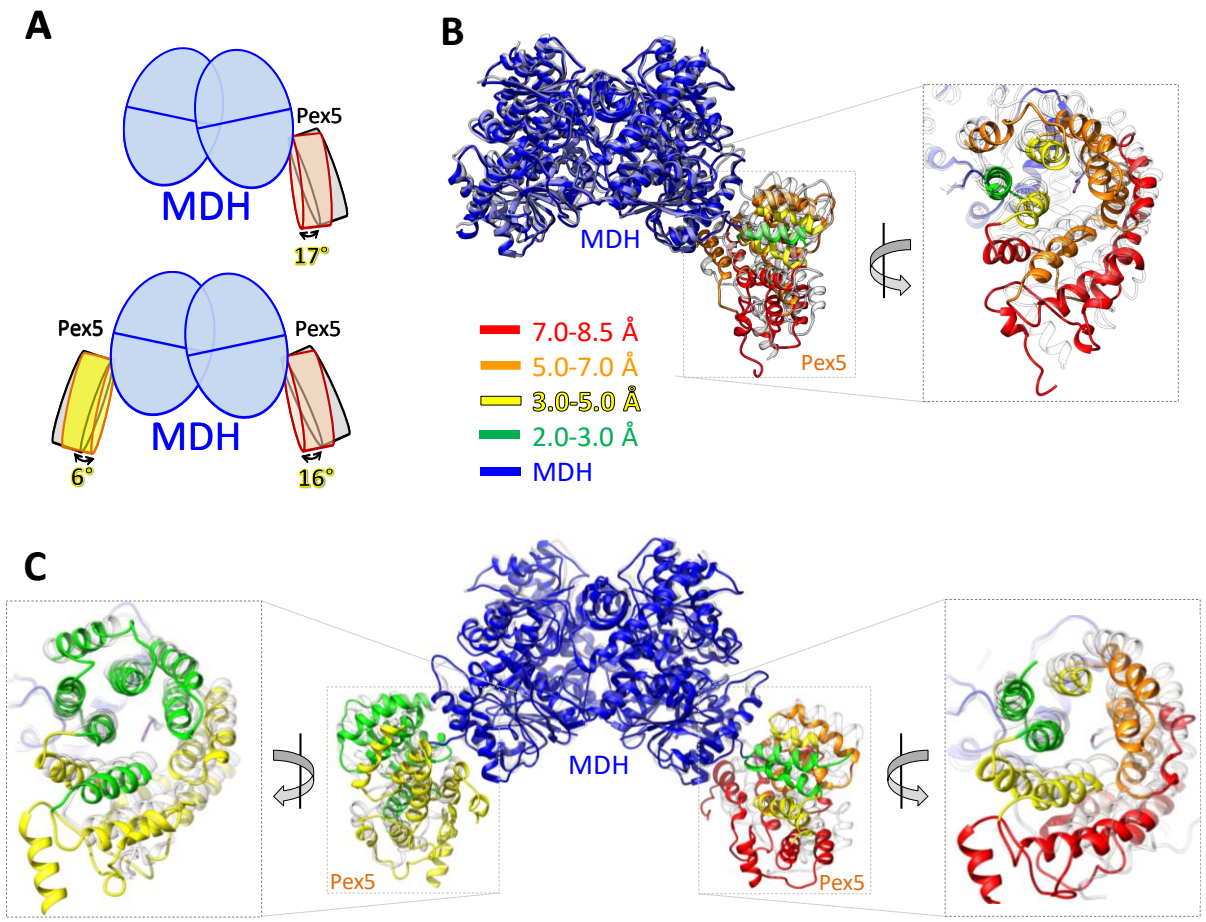

Figure 1. The Pex5-cargo interface accommodates significant conformational flexibility. (A) Schematic representation of angular movement (tilt) of Pex5 on MDH cargo in MP1 (upper panel) and MP2 (lower panel) structures. **(B, C)** Superimposed 3D structures of close/distal (colored/grey) conformations of MP1 **(B)** and MP2 **(C)** complex. Color codes in proximal confirmation represent the extent of movement between distal and proximal confirmations as depicted in inset. MDH is shown in blue in all panels. Pex5 is color coded according to the discussed features.

Pex5-binding on cargo is of dynamic nature

Recognition of the cargo by Pex5 is mediated *via* canonical PTS1 peptide interaction at the central cavity of TPR domain composed of 15 spirally aligned α-helices (Suppl. Mat. 8). It has been documented elsewhere that human and *Trypanosoma brucei* Pex5 TPR domain undergoes structural rearrangement adopting compact geometry upon PTS1 binding (*5, 6, 28*). The overall fold of *T. cruzi* Pex5 in our structures resembles the compact geometry observed in human (*6, 28*) and *T. brucei* Pex5 TPR (*5*) with average RMSD value of

~1.20 Å. As such, compaction of TPR domain upon PTS1 interaction seems a general, specie independent feature.

To facilitate cargo recognition, PTS1 extends beyond the globular structure of the cargo. This, in principle, should allow unrestrained conformational flexibility of Pex5 orientations relative to the cargo. Certain degree of flexibility was seen in the earlier crystal structure of human alanine-glyoxylate aminotransferase (AGT) complex with TPR domain of *Hs*Pex5 (*7, 8*) when the binding of two molecules of Pex5 at the AGT dimer were compared. However, crystals select for homogenous arrangements of components and thus, the structure may not have fully reflected the structural flexibility of the Pex5-cargo interface. Here we directly show that Pex5 is subject to a swinging motion at the surface of MDH cargo and the extent of the tilt is limited by secondary interactions between the cargo and Pex5. The 3DVA allowed to identify 9 and 11 clusters of particles for MP1 and MP2, respectively, spanning a continuum of the swinging motion of Pex5 relative to the cargo. The unbiased distribution of particles across the clusters suggests that none of the orientations is preferred.

The swinging movement of Pex5 can be described by two components, tilting and twisting. Pex5 oscillates between close and distal conformations with a tilt angle of 17° relative to the PTS1 axis (Fig. 1A; Suppl. Movies 1-7). While tilting, the Pex5 rigid body twists by about 13° relative to the axis roughly parallel to the TPR3 motif (Supp. Movie 8). Combined tilting and twisting motions bring radial displacement of Pex5 ranging between 3-8Å. TPR motifs 1, 2, 6 and 7 (residues 330-425, 527-640) are displaced further (by 5-8 Å) than the central TPR motifs, 3, 4 and 5 (residues 428-525), which are displaced by ~3.5 Å (Fig. 1B, 1C; Suppl. Movie. 1-8). The motion is almost identical in MP1 and MP2 structures. 3DVA analysis shows that the movement of two Pex5 molecules in MP2 structure is out of phase, that is, the movement of one component is independent of the other (Suppl. Movies 4, 5).

PTS1 independent, secondary cargo-Pex5 interactions

The swinging motion of Pex5 relative to MDH is characterized by significant dynamics, however is still restricted to a tilt angle of 17° and twist angle of 13°. This is

because PTS1 protrudes out of the globular structure of MDH only on a short linker, and the tilt of Pex5 is hindered by secondary (PTS1 independent) Pex5-MDH interactions. Analysis of the binding interface with PISA server identifies two additional sets of interactions between MDH and Pex5 (Fig. 2). First set of interactions, common to both close and distal conformations (MP1-c and MP1-d, respectively), involves an MDH loop encompassing residues 62-70 and a Pex5 region covering residues 439-444 – a connection between helices α6 and α7 within TPR3. The second set of interactions is observed only in the closed conformation. It involves MDH residues 142-145 and Pex5 helix α15 (residues, 625-633) downstream TPR7 motif (Fig. 2, Suppl. Mat. 8,9).

Interestingly, loop 62-70 is characteristically present only in the glycosomal isoform of MDH in *Trypanosoma*, and not in the cytosolic/mitochondrial isoforms or in homologues from other organisms (Suppl. Mat. 9), suggesting a specific role in glycosomal transport (*29*). To test the influence of identified sites on Pex5-cargo recognition, we evaluated the affinity of interaction surface mutants. The affinity of Pex5 for wild type MDH was estimated at K_d=504±150 nM by ITC (Table I). Deletion of the loop encompassing residues 63-70 in MDH resulted in no significant change in affinity, but was accompanied by a shift in the driving energetic component (Table I). While the affinity of wild type MDH was enthalpy driven, the binding of a loop deletion mutant is driven by entropy. Observed changes in the components of Gibbs free energy may be explained by loss of direct interactions of the loop and Pex5 compensated by increased dynamics of the loop deletion mutant containing complex (Table I). Alanine substitution of polar sidechains in Pex5 (R625A, D629A) predicted to participate in secondary interactions with the MDH motif 142-145 resulted in roughly 7-times increased affinity (Table I). These results collectively indicate that the secondary Pex5/cargo interactions are not optimized to increase affinity, but rather provide a steric hinderance which restricts the conformational flexibility.

A loop (residues 457-489) connecting TPR motif 3 and 4 is unstructured in available crystal structures of TPR domain of PEX5. The function of the loop is unknown, but following circumstantial evidence from this study suggests it may be involved in transient interaction with the cargo. The loop is not defined in our structure, but the structure indicates that the loop extends in a direction of a groove between MDH protomers. The said groove is deeper in glycosomal MDH compared to otherwise flat interface of cytosolic / mitochondrial MDHs

owned to a 62-70 insertion specifically found in the former molecule and forming a side of the groove. A weak map density is seen at the MDH groove in our structure of the complex – although not structurally interpretable, it may suggest transient orientation of the loop. To evaluate these assumptions, we tested the interaction of Pex5 partial loop deletion mutant with MDH. The affinity of the mutant for MDH was 10x higher compared to wild type Pex5 (Table I). At the same time the affinity of the mutant towards isolated PTS1 peptide dropped almost 4 times indicating that the increased affinity of the loop mutant for MDH is related to abolished unfavorable Pex5 loop - MDH interactions (Table I). To further evaluate the role of the loop we replaced a helix breaking proline (P490) residue initiating the loop with a residue affording less conformational strain at the backbone. The P490R mutant was characterized by three times lower affinity compared to the wild type again suggesting the involvement of the loop in transient Pex5 cargo interaction (Table I). Overall, these results suggest that the transient interactions of the loop restrict the dynamics of Pex5 at the cargo in concert with the other secondary interactions described above.

Finally, to determine the collective influence of secondary Pex5-cargo interactions we introduced a linker (GSGS) between PTS1 and the cargo to physically separate the surfaces of both molecules. The insertion mutant was characterized by 4 times higher affinity compared to the wild type (Table I). The affinity of the insertion mutant was comparable to that of an ARSKL peptide (PTS1 signal derived from MDH) indicating that the secondary interactions between the proteins were removed in the mutant (Table I). The above results collectively demonstrate that the PTS1 independent, secondary interactions between MDH and Pex5 restrain the conformational flexibility of Pex5 at the surface of the cargo while negatively affecting the affinity.

Noncanonical Pex5-Pex14 interactions

All 3DVA reconstructions were characterized by discernable, but poorly resolved density upstream of TPR domain of Pex5. Focused refinement resulted in a more detailed map accounting for a single Pex14 molecule bound at the Wxxx(F/Y) motif proximal to the TPR domain. Satisfactory rigid body fit of Pex14 structure (PDB id: 6ZFW) was obtained in the composite map encompassing the entire ternary complex (Suppl. Fig. S7).

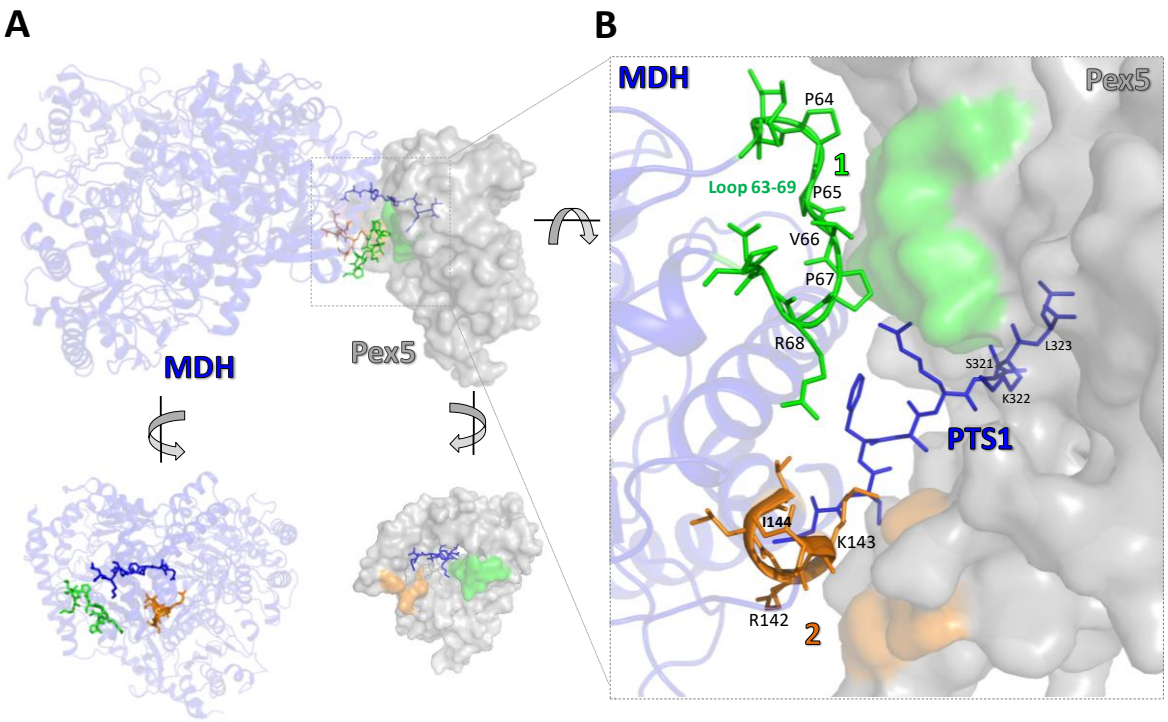

Figure 2. Secondary Pex5-cargo interactions. (A) Two non-canonical interactive surfaces (indicated by 1 and 2) between MDH and Cargo is shown by green and orange colors, respectively in addition to the canonical PTS1 (blue) interface. The MDH and Pex5 is shown as light blue ribbon and grey surface, respectively. (**B**) Close-up at the interaction site. Important residues discussed in the text are highlighted (stick model). Exemplified using MP1-c structure.

Table I. Mutational analysis of Pex5-cargo interface. Interaction of indicated mutants was characterized by Isothermal Titration Calorimetry (ITC).

Pex5	MDH	Affinity K_d [nM]	ΔH [kJ/mol]	-TΔS [kJ/mol]	N
WT	**WT**	504 ± 150	-26.8 ± 1.2	-9.2	0.47 ± 0.02
	GSGS	129 ± 33	-26.7 ± 0.4	-12.6	1.28 ± 0.01
	Δ(62-70)*	140 ± 58	-12.3 ± 0.8	-23.8	0.62 ± 0.03
	PTS1#	96 ± 30	-28.7 ± 0.6	-11.40	0.80 ± 0.01
R625A, D629A	**WT**	74 ± 28	-22.2 ± 0.5	-18.45	0.47 ± 0.01
P490R		1496 ± 394	-25.3 ± 1.5	-8.0	0.51 ± 0.02
Δ(470-480)		51 ± 22	-23.5 ± 0.6	-18.2	0.55 ± 0.01
	PTS1#	357 ± 76	-22.0 ± 0.4	-14.8	1.20 ± 0.02

* 62-KLPPVPRDP-70 loop was substituted with GS linker
#PTS1 peptide derived from MDH (NH_2-ARSKL-COOH)

The Pex14-Pex5 interface is composed of two interaction sites (Fig. 3). The canonical interaction involves Pex5 Wxxx(F/Y) motif binding at a hydrophobic groove on Pex14 surface (*14*). Along the canonical interaction, our structure reveals that helix α3 of Pex14 creates a number of contacts with 353-NNPYM-358 motif of Pex5 (Fig. 3; Suppl. Mat. 8 and 10). The

total buried surface area of Pex14-Pex5 interaction amounts to ~ 1300 $Å^2$ with only ~500 $Å^2$ contributed by the Wxxx(F/Y) motif and the rest by the noncanonical site suggesting significant contribution to affinity. The resolution of our structure at the interaction site is not high enough to clearly visualize the involvement of particular sidechains, but earlier crystallographic structures of Pex14 and separately of Pex5, together with modeling based on our low resolution map suggest the principal involvement of N353 and Y358 of Pex5, while P352 and P355 sustain the scaffold of the involved interhelix linker. The analysis further suggests the involvement of Q52 and N49 of Pex14. To evaluate the contribution of the noncanonical site to affinity we tested a number of mutants. The affinity (K_d) of Wxxx(F/Y) binding domain of Pex14 for truncated Pex5 containing a TPR domain and single proximal Wxxx(F/Y) site was estimated at 227 nM by ITC (Table II). Pex14 Q52A and N49A, Q52A mutants were designed to abolish presumable hydrogen bond interactions with Pex5, while A48F mutant was intended to introduce a steric clash. Unexpectedly, all tested mutants showed 7-18 times higher affinity compared to the wild-type (Table II) suggesting that the wild type interface is not optimized for affinity. Introduction of nonpolar patches in place of polar sidechains (N49A, Q52A) increased the affinity 18-fold. Enlarging the preexisting hydrophobic surface with A48F resulted in 7-fold affinity increase. Further probing the noncanonical interface, Pex5 Y358A and N353E mutants were respectively designed to abolish the presumed hydrophobic and electrostatic interactions with Pex14. P352A, P355A mutant was expected to compromise the scaffold of the interhelix linker involved in the noncanonical interaction. Again, the tested mutants of Pex5 showed 3-4 times higher affinity compared to the wild type. Replacing larger hydrophobic surface with a small sidechain (Y358A) resulted in 4-fold increase in affinity. Introduction of a charged sidechain at the center of noncanonical interaction surface (N353E) increased the affinity 3.5-fold. Even interfering with the scaffold supporting the noncanonical interaction surface on Pex5 (P352A, P355A) resulted in 3-fold affinity increase. These results collectively suggest that the noncanonical interaction of Pex14 and Pex5 is not optimized to positively contribute to the affinity.

To further verify the above conclusions, we tested the overall influence of noncanonical Pex14-Pex5 interactions on affinity by introducing a spacer between the TPR domain of Pex5 and the Wxxx(F/Y) binding site, intended to physically separate the

noncanonical interaction surfaces. The affinity of the insertion mutant (K_d=65nM) was 3.5 times higher compared to the wild type, again demonstrating that the interactions at the noncanonical site are not optimized to increase the affinity, but possibly to limit the conformational flexibility of the Pex14-Pex5 interface at the cost of affinity.

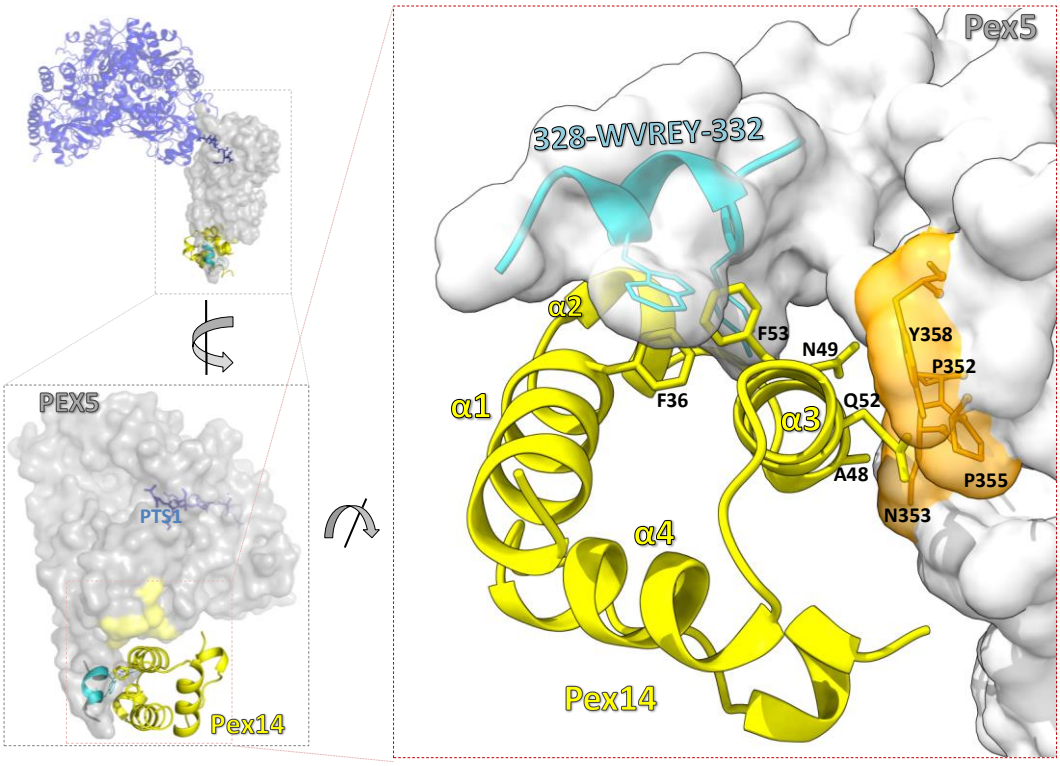

Figure 3. **Noncanonical interface of Pex14-Pex5.** (Left) Pex14 (yellow ribbon) interaction with Pex5 (surface model) in complex with MDH (dark blue) as seen in MP1P structure. (Right) Details of Pex14/Pex5 interface. Canonical docking of Pex5 Wxxx(F/Y) motif (cyan) at a groove on Pex14 NTD formed by α1 and α3 helices and noncanonical interaction of Pex14 α3 helix and 353-NNPYM-358 motif at the surface of Pex5. Important residues discussed in the text are highlighted (stick model).

Table II. Mutational analysis of Pex14-Pex5 interface. Interaction of indicated mutants was characterized by Isothermal Titration Calorimetry (ITC).

Pex5	Pex14	Affinity K_d [nM]	ΔH [kJ/mol]	-TΔS [J/molK]	N
WT	**WT**	227 ± 24	-37.1±0.3	-0.81	0.726 ± 0.004
	Q52A	18 ± 4	-47.8±0.3	3.55	0.619 ± 0.002
	N49A, Q52A	13 ± 6	-35.3±0.5	-9.74	0.732 ± 0.006
	A48F	33 ± 5	-49.2±0.3	6.49	0.689 ± 0.002
Y358A	**WT**	57 ± 6	-57.5±0.3	16.09	0.729 ± 0.002
P352A, P355A		79 ± 10	-45.7±0.3	5.18	0.932 ± 0.003
N353E		65 ± 7	-52.1±0.3	11.03	0.689 ± 0.002
GSSG		65 ± 8	-47.1±0.3	6.03	0.702 ± 0.003

DISCUSSION

Specialized peroxisomes, known as glycosomes, compartmentalize glycolytic reactions in *Trypanosoma.* Glycosomal malate dehydrogenase (MDH) is a crucial enzyme auxiliary to glycolysis which uses nicotinamide adenine dinucleotide (NAD) cofactor to catalyse reversible oxidation / reduction maintaining the pool of malate / oxaloacetate and NAD^+ / NADH within the glycosome (*30, 31*). We demonstrate that Pex5-MDH complex is characterized by significant structural dynamics, constrained by secondary protein-protein interactions. The flexibility of the interface is not unexpected since Pex5 binds to diverse cargos. In fact, it has been demonstrated that nonperoxisomal proteins may be efficiently delivered to the peroxisome by appending their sequence with PTS1. Such result indicates that the interaction of PTS1 and the Pex5 TPR domain is sufficient for efficient delivery and no additional interactions are necessary. Yet, an earlier study on human alanine-glyoxylate aminotransferase demonstrated importance of secondary interactions at the Pex5-cargo interface (*8*), though the static crystal structure did account for the dynamics of the interface. We demonstrate that secondary interactions at MDH-Pex5 interface do not add to the affinity, but rather restrict the cargo dynamics at the cost of affinity. PTS1 extends only just above the surface of MDH which is not favorable in terms of recognition kinetics. We demonstrate that the addition of short linker of four amino acids extending PTS-1 away from MDH surface indeed provides better affinity by releasing the restrains induced by secondary interactions. Nevertheless, the shorter linker favoring the secondary interactions has been selected during the course of evolution suggesting the importance of restrained conformational dynamics at MDH-Pex5 interface. The characteristic insertion (residues 62-70) of glycosomal MDH provides enthalpic contribution to the interface at the same time sterically limiting the extent of Pex5 swinging motion. Pex5, in turn, contains an unstructured loop (residues 457-489) extending in the direction of the MDH further restricting the conformational dynamics as demonstrated by 10x increased affinity of loop deletion mutant. We speculate that defined conformational flexibility may finetune the pore translocation and that the moderated Pex5-cargo affinity may support the cargo release in the peroxisome. However, verification of this speculation must await better understanding of related processes.

The cryo-EM reconstitution and the crystal structure of MDH tetramer indicate unobstructed accessibility of PTS1 signal on all protomers. Yet, complexes containing two molecules of Pex5 located on two adjacent protomers, but not on two opposed protomers, were only detected, positioning the unstructured Pex5 NTD towards the same pole of MDH. The reason for this selected topology is unclear, since no interaction between Pex5 molecules is seen. It is also unknown if occupation of more than single Pex5 site is needed for translocation, but the piggybacking of isoforms within heteromultimeric complexes suggests that not all the Pex5 interaction sites need saturation (*32, 33*).

Pex5 contains an unstructured, N-terminal domain encompassing a number of Pex14 binding sites. It has been hypothesized earlier that the binding of Pex14 to Pex5-cargo complex induces cargo release (*34*). The present cryo-EM structure of MDH-Pex5-Pex14 indicates that binding of the N-terminal Pex14 domain alone is not sufficient for the release of the cargo from Pex5. It has also been reported earlier that saturation of Pex14 sites results in a rigidification of the complex structure, but this conclusion is not supported by our study. Although full length Pex5 was used for complex reconstitution, the density is resolved only shortly beyond the Wxxx(F/Y) motif proximal to the TPR domain. Prior crystal structures of the TPR domain of Pex5 revealed a compact snail-shaped PTS1 binding site arrangement, but the Pex14 binding sites were not resolved. We demonstrate here that the proximal Wxxx(F/Y) site is embedded in a helical motif extending beyond the TPR domain. Pex14 docking at the diaromatic motif shows canonical features investigated earlier by protein crystallography, but the rigid structure of the helix connecting the Wxxx(F/Y) site and TPR domain imposes noncanonical interactions of α3 helix of Pex14 and TPR4 motif of Pex5. Interestingly, mutagenesis of the interaction site demonstrates incompatibility of the contact surfaces in the wild type proteins. Substitution of long chain hydrogen bond donors within the interaction site of Pex14 with alanine or replacement of prolines maintaining the scaffold of the interaction site of Pex5 and other tested mutations at the interaction site consistently result in increased affinity of the mutants. As such, the Pex14 α3 helix – Pex5 TPR4 motif interface exemplifies a rare instance of protein-protein interaction site which limits the dynamics of the system at the cost of overall affinity.

T. cruzi is responsible for Chagas disease, a neglected tropical disease affecting millions of people in Central America (*25*). The lifelong Chagas disease is characterized by

gradual deterioration of heart and gastrointestinal tract eventually leading to death (*35-37*). Limited treatment options are available and threatened by increasing resistance (*38-40*). The unique feature of *Trypanosoma* is to compartmentalize glycolytic enzymes into peroxisome like organelles known as glycosomes. Mislocalization of glycolytic enzymes to the cytoplasm results in metabolic catastrophe and death, hence the Pex import is the promising drug target in trypanosomiases (*41-44*). Thereby, the presently described structure of Pex ternary complex can provide platform to the drug development efforts in future.

In summary, this study provided insight into structural organization of the translocating complex of the peroxisomal protein import system. Structural dynamics and the secondary interactions limiting the extent of the dynamics of cargo-Pex5 interface were characterized. A noncanonical site of interaction was identified at Pex14 – Pex5 interface and it was shown that the site limits the affinity of the primary Pex5-PTS1 binding.

MATERIAL AND METHODS

Protein expression and purification

Genes encoding *Trypanosoma cruzi* MDH, Pex5, truncated Pex5 (residues 314-666, Pex5 TPR+) and Pex14 N-terminal domain (residues, 21 to 85, Pex14 NTD) were *de novo* synthesized with N-terminal 6×His, 6×His and 6×His-TEVsite tags, respectively. Genes were cloned in pET24(+) vector using NdeI and XhoI restriction sites. Recombinant vectors were transformed individually in *Escherichia coli* BL21 (DE3) for over-expression. Proteins were purified by Ni-affinity (Ni-NTA) and size exclusion chromatography (SEC). Purified Pex14 was subjected to TEV protease treatment to remove 6×His-tag. Mutations were introduced by site directed mutagenesis and the mutants were purified as wild type proteins.

In vitro reconstitution and purification of the ternary complex

Purified MDH, Pex5 (or alternatively Pex5 TPR+) and Pex14 NTD were mixed at 1:4:12 (MDH tetramer:Pex5:Pex14; 1:4:4 for Pex5 TPR+) molar stoichiometry and incubated overnight at 4°C. The complex was separated from remaining individual components by SEC

using Superose® 6 10/300. Complex formation was analysed by native-PAGE, SDS-PAGE, DLS and SEC-MALS.

Sample preparation and cryo-EM data acquisition

Purified ternary complex was vitrified on holey-carbon grids (Quantifoil R 2/1) using FEI Vitrobot Mark IV. Carbon grids were glow-discharged at 8 mA for 70 sec using LEICA EM ACE200 glow-discharger. Glow-discharged grids were loaded with 3 µL of sample, blotted (blot time: 5 sec; blot force: 5 units) and flash-frozen by plunging into liquid ethane. Frozen-grids were screened for the quality of ice and contrast on 200 kV Glacios microscope equipped with Falcon 4 detector prior to data collection on 300 kV Krios G3i Cryo-TEM microscope equipped with Falcon 4 detector at a magnification of ×105k. Each exposure was recorded into 40 dose-fractioned frames with total electron dose of 42.25 $e^-/Å^2$. Grid screening and data collection was performed at cryo-EM facility at the Solaris synchrotron in Krakow, Poland.

Cryo-EM data processing

Data was processed using *cryoSPARC 3.3.1* (*45*). Micrographs were motion corrected and subjected to contrast transfer function (CTF) estimation using *patch motion correction (multi)* and *patch CTF estimation (multi)* jobs, respectively. Protein-particles were picked on a subset of micrographs using *blob-picker*. Picked particles were subjected to template-free 2D classification to generate initial templates. The generated 2D templetes were used to pick particles from the whole dataset by *template-picker*. A total of 315,016 particles were picked from 8,169 micrographs and again subjected to iterative template-free 2-D classification. 273,101 particles were finally selected using 2D classes and subjected to *ab-initio* 3D reconstruction, heterogeneous refinement and homogenous refinement in order to get compositionally differing reconstruction maps. In order to assess conformational heterogeneity, the particle stack (273,101 particles) was subjected to 3-D variability analysis (3DVA) in *cluster* output mode (*26*). Selected particle clusters and associated volume maps were individually subjected to *non-uniform homogenous refinement* in order to reconstitute individual 3D maps representing different compositional and conformational states of the complex. Furthermore, to deal with structural flexibility in Pex region, 92,488 particles were selected from 3DVA clusters and subjected to focused refinement of MDH and Pex regions

of map using local masks. Locally refined maps were combined in UCSF chimera to generate final composite map. Density maps were further sharpened using sharpening tool of cryoSPARC. Overall quality of cryo-EM data and data-processing workflow is depicted in Supp. Mat. 1- 7 and Supp. Table S1.

Model building and refinement

Crystal structure of MDH (PDB id: 7QOZ) and the structure of *T. cruzi* Pex5 TPR domain (PDB id: 7ZT1) were used to fit MP1 and MP2 maps using *Dock in map* program of Phenix suite (*46*). Docked models were subjected to flexible fitting into the map using namdinator web-server (*47*). Fitted models were refined against the map by iterative cycles of automatic refinement using phenix real-space refinement (*48*) and interactive refinement using COOT (*49*) until reasonable geometry and map-to-model correlation were achieved. After refinement of MDH and Pex5 model against maps, *T. cruzi* Pex14 crystal structure (PDB id: 6ZFW) was used for fitting in MP1P map using *Dock in map* program (Phenix suit) and trimmed. Pex14 was not further refined against the map. Validation of model and model *vs*. data for all structures are summarized in Supp. Mat. 3- 7 and Supp. Table S1.

Data analysis and representation

The analysis, manipulation and representation of cryo-EM maps and 3D structures were performed using COOT (*49*), PyMOL (Schrödinger, LLC), UCSF chimera (*50*) and chimeraX (*51*). Sequence alignments were performed and presented using MEGA X software and ESpript server (*52*), respectively.

Isothermal Titration Calorimetry (ITC)

ITC measurements were performed in 20 mM sodium phosphate buffer containing 100 mM NaCl at pH 6.5 (Pex5-Pex14 interaction) or 100 mM Hepes buffer containing 150 mM NaCl and 2 mM β-mercaptoethanol at pH 7.5 (MDH-Pex5 interaction) using a Nano ITC 2G (TA Instruments). Before the experiments, proteins were extensively dialyzed against the relevant buffer. The binding experiment involved 5 µL injections of Pex14 solution (600 µM) or Pex5 (250 µM) into the calorimeter cell containing Pex5 (35 µM) or MDH (25 µM), respectively. Injections were performed at 300 s intervals. All experiments were conducted at 25 °C with a stirring rate of 250 rpm. The heat of dilution was determined by titration of Pex14 (Pex5-Pex14) or Pex5 (MDH-Pex5) to protein-free buffer. The data were analyzed

using NanoAnalyze software (TA instruments). The binding stoichiometry (N), the dissociation constant (K_d) and the enthalpy change (ΔH) were obtained from fitting the data with 1:1 binding model. The Gibbs free energy (ΔG) and change in entropy (ΔS) were calculated using $-RT \ln Kd = \Delta G = \Delta H - T\Delta S$, where R is the gas constant and T is the absolute temperature.

SEC-MALS

Protein samples (4mg/mL; 80 µL) were separated on Superdex 200 Increase 10/300 GL Tricoedn column (GE Healthcare) in 20 mM Hepes containing 150 mM KCl, 5 mM $MgCl_2$, 2 mM β-mercaptoethanol, pH 7.5 using NGC Scout 10 Medium-Pressure Liquid Chromatography System (Bio-Rad) equipped with RefractoMax 520 Refractive Index Detector (ERC Inc.) and miniDAWN TREOS multi-angle light scattering system (Wyatt). BSA was used as the isotropic scatterer for detector normalization (4.5 mg/mL). The molar masses were calculated with the ASTRA 7.1.4.8 software.

DLS

The DLS was determined using Zetasizer Nano ZS (Malvern). MDH, Pex5 and their complexes were used at the concentration of 1 mg/mL in the SEC buffers. Protein samples were equilibrated at 10°C for 2.5 min and measured with standard settings for Tris-HCl buffer.

Data availability

Density maps of complexes, MP1-c, MP1-d, MP2-c, MP2-d and MP1P were deposited to the electron microscopy database (EMBD) with accession ids, 40003, 40008, 40031, 40032 and 40056, respectively. Refined 3D-structure coordinates of complexes, MP1-c, MP1-d, MP2-c, MP2-d and MP1P were deposited to the protein data bank (PDB) with accession ids, 8GGD, 8GGH, 8GH2, 8GH3 and 8GI0.

ACKNOWLEDGEMENTS

This work was supported in parts by grants 2017/26/M/NZ1/00797 (construct preparation, crystal structure of selected components) and 2020/39/B/NZ1/01551 (remaining experiments), both to GD, from the Polish National Science Centre. RS was a recipient of NAWA Ulam scholarship. We thank Marcin Jaciuk, Katarzyna Pustelny and Rahul Mehta from Malopolska Centre of Biotechnology of the Jagiellonian University, and Grzegorz Popowicz, Valeira Napolitano and Florian Schlauderer from Helmholtz Center in Munich for valuable discussion, assistance in experiments and providing materials. We acknowledge the access to cryogenic electron microscope at National Synchrotron Radiation Centre SOLARIS supported under contract nr 1/SOL/2021/2 from Polish Ministry of Education and Science. We thank Michal Rawski and Paulina Indyka for assistance. This research was supported in part by PLGrid Infrastructure. We thank Klemens Noga from AGH Cyfronet for excellent assistance. We thank the MCB structural biology core facility (supported by the TEAM TECH CORE FACILITY/2017-4/6 grant from Foundation for Polish Science) for providing instruments and support. We acknowledge the Core Facility for Crystallography and Biophysics, University of Warsaw (supported by the Foundation for Polish Science under the European Regional Development Fund, TEAM TECH Core Facility POIR.04.04.00-00-31DF/17) for valuable support. The open-access publication of this article was funded by the Priority Research Area BioS under the program “Initiative of Excellence - Research University” at the Jagiellonian University in Krakow.

CONTRIBUTIONS

RS – devised expression and purification protocols, reconstituted the complex, solved the cryo-EM structures, analysed the data, wrote the manuscript, prepared figures.

AB – expressed proteins, performed biochemical assays, analysed the results, contributed to writing of parts of the manuscript.

M. J-R. - performed isothermal calorimetry (ITC) assay and analysed the results.

OL, SP, TS – expressed and purified proteins, performed biochemical assays.

GD – obtained funding, coordinated the project, discussed the results, wrote the manuscript.

COFLICT OF INTEREST

Authors declare that there is no conflict of interest.

REFERENCES

1. R. J. Wanders, H. R. Waterham, Biochemistry of mammalian peroxisomes revisited. *Annual review of biochemistry* **75**, 295-332 (2006).
2. M. Islinger, A. Voelkl, H. D. Fahimi, M. Schrader, The peroxisome: an update on mysteries 2.0. *Histochemistry and cell biology* **150**, 443-471 (2018).
3. B. M. Goldman, G. Blobel, Biogenesis of peroxisomes: intracellular site of synthesis of catalase and uricase. *Proceedings of the National Academy of Sciences* **75**, 5066-5070 (1978).
4. T. Lanyon-Hogg, S. L. Warriner, A. Baker, Getting a camel through the eye of a needle: the import of folded proteins by peroxisomes. *Biology of the Cell* **102**, 245-263 (2010).
5. P. Sampathkumar, C. Roach, P. A. Michels, W. G. Hol, Structural insights into the recognition of peroxisomal targeting signal 1 by Trypanosoma brucei peroxin 5. *Journal of Molecular Biology* **381**, 867-880 (2008).
6. W. A. Stanley, F. V. Filipp, P. Kursula, N. Schüller, R. Erdmann, W. Schliebs, M. Sattler, M. Wilmanns, Recognition of a functional peroxisome type 1 target by the dynamic import receptor pex5p. *Molecular cell* **24**, 653-663 (2006).
7. K. Fodor, J. Wolf, R. Erdmann, W. Schliebs, M. Wilmanns, Molecular requirements for peroxisomal targeting of alanine-glyoxylate aminotransferase as an essential determinant in primary hyperoxaluria type 1. *PLoS biology* **10**, e1001309 (2012).
8. K. Fodor, J. Wolf, K. Reglinski, D. M. Passon, Y. Lou, W. Schliebs, R. Erdmann, M. Wilmanns, Ligand-induced compaction of the PEX5 receptor-binding Cavity impacts protein import efficiency into peroxisomes. *Traffic* **16**, 85-98 (2015).
9. Y. Gao, M. L. Skowyra, P. Feng, T. A. Rapoport, Protein import into peroxisomes occurs through a nuclear pore–like phase. *Science* **378**, eadf3971 (2022).
10. J. r. Saidowsky, G. Dodt, K. Kirchberg, A. Wegner, W. Nastainczyk, W.-H. Kunau, W. Schliebs, The di-aromatic pentapeptide repeats of the human peroxisome import receptor PEX5 are separate high affinity binding sites for the peroxisomal membrane protein PEX14. *Journal of Biological Chemistry* **276**, 34524-34529 (2001).
11. H. Otera, K. Setoguchi, M. Hamasaki, T. Kumashiro, N. Shimizu, Y. Fujiki, Peroxisomal targeting signal receptor Pex5p interacts with cargoes and import machinery components in a spatiotemporally differentiated manner: conserved Pex5p WXXXF/Y motifs are critical for matrix protein import. *Molecular and cellular biology* **22**, 1639-1655 (2002).
12. J. Choe, J. Moyersoen, C. Roach, T. L. Carter, E. Fan, P. A. Michels, W. G. Hol, Analysis of the sequence motifs responsible for the interactions of peroxins 14 and 5, which are involved in glycosome biogenesis in Trypanosoma brucei. *Biochemistry* **42**, 10915-10922 (2003).

13. C. Williams, M. van den Berg, B. Distel, Saccharomyces cerevisiae Pex14p contains two independent Pex5p binding sites, which are both essential for PTS1 protein import. *FEBS letters* **579**, 3416-3420 (2005).
14. C. Neufeld, F. V. Filipp, B. Simon, A. Neuhaus, N. Schüller, C. David, H. Kooshapur, T. Madl, R. Erdmann, W. Schliebs, Structural basis for competitive interactions of Pex14 with the import receptors Pex5 and Pex19. *The EMBO Journal* **28**, 745-754 (2009).
15. A. Barros-Barbosa, M. J. Ferreira, T. A. Rodrigues, A. G. Pedrosa, C. P. Grou, M. P. Pinto, M. Fransen, T. Francisco, J. E. Azevedo, Membrane topologies of PEX 13 and PEX 14 provide new insights on the mechanism of protein import into peroxisomes. *The FEBS journal* **286**, 205-222 (2019).
16. N. Shimizu, R. Itoh, Y. Hirono, H. Otera, K. Ghaedi, K. Tateishi, S. Tamura, K. Okumoto, T. Harano, S. Mukai, The peroxin Pex14p: cDNA cloning by functional complementation on a Chinese hamster ovary cell mutant, characterization, and functional analysis. *Journal of Biological Chemistry* **274**, 12593-12604 (1999).
17. C. Brocard, G. Lametschwandtner, R. Koudelka, A. Hartig, Pex14p is a member of the protein linkage map of Pex5p. *The EMBO Journal* **16**, 5491-5500 (1997).
18. M. E. Oliveira, C. Reguenga, A. M. Gouveia, C. P. Guimarães, W. Schliebs, W.-H. Kunau, M. T. Silva, C. Sá-Miranda, J. E. Azevedo, Mammalian Pex14p: membrane topology and characterisation of the Pex14p–Pex14p interaction. *Biochimica et Biophysica Acta (BBA)-Biomembranes* **1567**, 13-22 (2002).
19. G. K. Will, M. Soukupova, X. Hong, K. S. Erdmann, J. A. Kiel, G. Dodt, W.-H. Kunau, R. Erdmann, Identification and characterization of the human orthologue of yeast Pex14p. *Molecular and cellular biology* **19**, 2265-2277 (1999).
20. K. Niederhoff, N. M. Meindl-Beinker, D. Kerssen, U. Perband, A. Schäfer, W. Schliebs, W.-H. Kunau, Yeast Pex14p possesses two functionally distinct Pex5p and one Pex7p binding sites. *Journal of Biological Chemistry* **280**, 35571-35578 (2005).
21. P. Lill, T. Hansen, D. Wendscheck, B. U. Klink, T. Jeziorek, D. Vismpas, J. Miehling, J. Bender, A. Schummer, F. Drepper, W. Girzalsky, B. Warscheid, R. Erdmann, C. Gatsogiannis, Towards the molecular architecture of the peroxisomal receptor docking complex. *Proc Natl Acad Sci U S A* **117**, 33216-33224 (2020).
22. Y. Gao, M. L. Skowyra, P. Feng, T. A. Rapoport, Protein import into peroxisomes occurs through a nuclear pore-like phase. *Science* **378**, eadf3971 (2022).

23. K. Shiozawa, P. V. Konarev, C. Neufeld, M. Wilmanns, D. I. Svergun, Solution structure of human Pex5· Pex14· PTS1 protein complexes obtained by small angle X-ray scattering. *Journal of Biological Chemistry* **284**, 25334-25342 (2009).
24. P. Lill, T. Hansen, D. Wendscheck, B. U. Klink, T. Jeziorek, D. Vismpas, J. Miehling, J. Bender, A. Schummer, F. Drepper, Towards the molecular architecture of the peroxisomal receptor docking complex. *Proceedings of the National Academy of Sciences* **117**, 33216-33224 (2020).
25. J. A. Pérez-Molina, I. Molina, Chagas disease. *The Lancet* **391**, 82-94 (2018).
26. A. Punjani, D. J. Fleet, 3D variability analysis: Resolving continuous flexibility and discrete heterogeneity from single particle cryo-EM. *Journal of Structural Biology* **213**, 107702 (2021).
27. L. Emmanouilidis, M. Gopalswamy, D. M. Passon, M. Wilmanns, M. Sattler, Structural biology of the import pathways of peroxisomal matrix proteins. *Biochim Biophys Acta* **1863**, 804-813 (2016).
28. G. J. Gatto, B. V. Geisbrecht, S. J. Gould, J. M. Berg, Peroxisomal targeting signal-1 recognition by the TPR domains of human PEX5. *Nature structural biology* **7**, 1091-1095 (2000).
29. R. R. Sonani, K. Kurpiewska, K. Lewiński, G. Dubin, Distinct sequence and structural feature of trypanosoma malate dehydrogenase. *Biochemical and Biophysical Research Communications* **557**, 288-293 (2021).
30. G. R. Hunter, U. Hellman, J. J. Cazzulo, C. Nowicki, Tetrameric and dimeric malate dehydrogenase isoenzymes in Trypanosoma cruzi epimastigotes. *Molecular and Biochemical Parasitology* **105**, 203-214 (2000).
31. P. Minarik, N. Tomaskova, M. Kollarova, M. Antalik, Malate dehydrogenases-structure and function. *General physiology and biophysics* **21**, 257-266 (2002).
32. S. Thoms, Import of proteins into peroxisomes: piggybacking to a new home away from home. *Open Biol* **5**, (2015).
33. S. Gabay-Maskit, L. D. Cruz-Zaragoza, N. Shai, M. Eisenstein, C. Bibi, N. Cohen, T. Hansen, E. Yifrach, N. Harpaz, R. Belostotsky, A piggybacking mechanism enables peroxisomal localization of the glyoxylate cycle enzyme Mdh2 in yeast. *Journal of cell science* **133**, jcs244376 (2020).
34. M. O. Freitas, T. Francisco, T. A. Rodrigues, I. S. Alencastre, M. P. Pinto, C. P. Grou, A. F. Carvalho, M. Fransen, C. Sá-Miranda, J. E. Azevedo, PEX5 protein binds monomeric catalase blocking its tetramerization and releases it upon binding the N-terminal domain of PEX14. *Journal of biological chemistry* **286**, 40509-40519 (2011).

35. R. B. De Oliveira, L. E. A. Troncon, R. O. Dantas, U. G. Meneghelli, Gastrointestinal manifestations of Chagas' disease. *The American journal of gastroenterology* **93**, 884-889 (1998).

36. M. C. P. Nunes, W. Dones, C. A. Morillo, J. J. Encina, A. L. Ribeiro, C. o. C. D. o. t. I. S. o. Cardiology, Chagas disease: an overview of clinical and epidemiological aspects. *Journal of the American College of Cardiology* **62**, 767-776 (2013).

37. N. M. Matsuda, S. M. Miller, P. R. B. Evora, The chronic gastrointestinal manifestations of Chagas disease. *Clinics* **64**, 1219-1224 (2009).

38. S. L. De Castro, The challenge of Chagas' disease chemotherapy: an update of drugs assayed against Trypanosoma cruzi. *Acta tropica* **53**, 83-98 (1993).

39. Y. Jackson, B. Wyssa, F. Chappuis, Tolerance to nifurtimox and benznidazole in adult patients with chronic Chagas' disease. *Journal of Antimicrobial Chemotherapy* **75**, 690-696 (2020).

40. S. R. Wilkinson, M. C. Taylor, D. Horn, J. M. Kelly, I. Cheeseman, A mechanism for cross-resistance to nifurtimox and benznidazole in trypanosomes. *Proceedings of the National Academy of Sciences* **105**, 5022-5027 (2008).

41. J. Moyersoen, J. Choe, E. Fan, W. G. Hol, P. A. Michels, Biogenesis of peroxisomes and glycosomes: trypanosomatid glycosome assembly is a promising new drug target. *FEMS microbiology reviews* **28**, 603-643 (2004).

42. M. Dawidowski, L. Emmanouilidis, V. Kalel, K. Tripsianes, K. Schorpp, K. Hadian, M. Kaiser, P. Mäser, M. Kolonko, S. Tanghe, Inhibitors of PEX14 disrupt protein import into glycosomes and kill Trypanosoma parasites. *Science* **355**, 1416-1420 (2017).

43. M. Dawidowski, V. C. Kalel, V. Napolitano, R. Fino, K. Schorpp, L. Emmanouilidis, D. Lenhart, M. Ostertag, M. Kaiser, M. Kolonko, Structure–activity relationship in pyrazolo [4, 3-c] pyridines, first inhibitors of PEX14–PEX5 protein–protein interaction with trypanocidal activity. *Journal of medicinal chemistry* **63**, 847-879 (2019).

44. V. Napolitano, P. Mróz, M. Marciniak, V. C. Kalel, C. A. Softley, J. D. J. Olmos, B. G. Tippler, K. Schorpp, S. Rioton, T. Fröhlich, Structure-based design, synthesis and evaluation of a novel family of PEX5-PEX14 interaction inhibitors against Trypanosoma. *European Journal of Medicinal Chemistry* **243**, 114778 (2022).

45. A. Punjani, J. L. Rubinstein, D. J. Fleet, M. A. Brubaker, cryoSPARC: algorithms for rapid unsupervised cryo-EM structure determination. *Nature Methods* **14**, 290-296 (2017).

46. D. Liebschner, P. V. Afonine, M. L. Baker, G. Bunkóczi, V. B. Chen, T. I. Croll, B. Hintze, L.-W. Hung, S. Jain, A. J. McCoy, Macromolecular structure determination using X-rays, neutrons

and electrons: recent developments in Phenix. *Acta Crystallographica Section D: Structural Biology* **75**, 861-877 (2019).

47. R. T. Kidmose, J. Juhl, P. Nissen, T. Boesen, J. L. Karlsen, B. P. Pedersen, Namdinator–automatic molecular dynamics flexible fitting of structural models into cryo-EM and crystallography experimental maps. *IUCrJ* **6**, 526-531 (2019).
48. P. V. Afonine, B. K. Poon, R. J. Read, O. V. Sobolev, T. C. Terwilliger, A. Urzhumtsev, P. D. Adams, Real-space refinement in PHENIX for cryo-EM and crystallography. *Acta Crystallographica Section D: Structural Biology* **74**, 531-544 (2018).
49. P. Emsley, K. Cowtan, Coot: model-building tools for molecular graphics. *Acta Cryst D* **60**, 2126-2132 (2004).
50. E. F. Pettersen, T. D. Goddard, C. C. Huang, G. S. Couch, D. M. Greenblatt, E. C. Meng, T. E. Ferrin, UCSF Chimera—a visualization system for exploratory research and analysis. *Journal of computational chemistry* **25**, 1605-1612 (2004).
51. T. D. Goddard, C. C. Huang, E. C. Meng, E. F. Pettersen, G. S. Couch, J. H. Morris, T. E. Ferrin, UCSF ChimeraX: Meeting modern challenges in visualization and analysis. *Protein Sci* **27**, 14-25 (2018).
52. X. Robert, P. Gouet, Deciphering key features in protein structures with the new ENDscript server. *Nucleic Acids Research* **42**, W320-W324 (2014).